Journal of Alloys and Compounds 862 (2021) 158020

Contents lists available at ScienceDirect

Journal of Alloys and Compounds

journal homepage: www.elsevier.com/locate/jalcom

Electronic and thermodynamic properties of lanthanum tetraboride on low-temperature experimental and *ab-initio* calculation data

G. Surucu[a,b], H. Ozısık[c], E. Deligoz[c], I.R. Shein[d], A.V. Matovnikov[e], N.V. Mitroshenkov[e], A.V. Morozov[f], V.V. Novikov[e,*]

[a] Middle East Technical University, Department of Physics, Ankara 06800, Turkey
[b] Department of Electric and Energy, Ahi Evran University, Kirsehir 40100, Turkey
[c] Aksaray University, Department of Physics, 68100 Aksaray, Turkey
[d] Institute of Solid State Chemistry, Ural Branch of the Russian Academy of Sciences, 91 Pervomayskaya, 620990 Ekaterinburg, Russia
[e] Bryansk Physical Laboratory, Petrovsky Bryansk State University, 14 Bezhitskaya, 241037 Bryansk, Russia
[f] Department of Physics, Russian Timiryazev State Agrarian University, 49 Timiryazevskaya St., 127550 Moscow, Russia

ARTICLE INFO

Article history:
Received 29 November 2019
Received in revised form 13 November 2020
Accepted 16 November 2020
Available online 23 November 2020

Keywords:
Tetraborides
First-principles calculations
Electronic properties
Phonon spectrum
Thermodynamic properties
Low temperature

ABSTRACT

The characteristics of the electronic and phonon subsystems of lanthanum tetraboride (LaB_4) studied using first-principles calculations. The calculated lattice parameters, as well as the positions of atomic, are satisfactorily consistent with the experimental data. The partial densities of states, band structure, Fermi surface, phonon dispersion curve of LaB_4 are calculated and analysed. The reliability of the calculation results is confirmed by a satisfactory agreement between the calculated thermodynamic parameters of LaB_4 (temperature changes in heat capacity, entropy, Grüneisen parameter and volume modulus) with experimental data.

1. Introduction

The study of rare-earth (RE) tetraborides, RB_4 (where R is a rare-earth metal), is of considerable scientific interest due to the peculiarity of their crystal structure and transitions to a magnetically ordered state at low temperature [1–8]. For a detailed study of the properties of the magnetic subsystems of RE tetraborides, it is necessary to be able to separate the magnitude of the magnetic contribution to the physical characteristics of borides from their full values. This is usually achieved by comparing the physical characteristics of magnetic substances with similar values for their isostructural analogues. For heavy RE tetraborides (Gd–Lu), this analogue is LuB_4. For the tetraborides with light REs (Ce–Eu), it is LaB_4.

Lanthanum tetraboride (LaB_4), like other RE tetraborides, crystallises into a tetragonal structure with space group P4/mbm. There are four formula units per unit cell [1]. The boron sublattice of tetraborides contains structural elements of both RB_2 diborides (a chain of boron atoms) and RB_6 hexaborides (B_6 octahedra). Strong covalent bonds in the boron sublattice provide the tetraborides with high hardness values and melting points. RE atoms are located between the distorted heptagonal rings of the boron atoms, forming the so-called frustrated Shastry-Sutherland lattice [9], which is responsible for the specific anomalies of the magnetic and thermodynamic properties of RE tetraborides at low temperatures [5,10–13].

The analysis of the experimental temperature dependencies of the specific heat $C_v(T)$ and unit cell volume $V_u(T)$ of LaB_4 [14] in the simple Debye-Einstein approximation showed that both dependencies can be satisfactorily approximated by the sum of the specific heat of the electron gas, with two Debye contributions C_{D1} and C_{D2} (θ_{D1} = 420 K and θ_{D2} = 230 K), as well as two Einstein components C_{E1} and C_{E2} (θ_{E1} = 890 K and θ_{E2} = 177 K). At the lowest temperatures, the main contribution to the heat capacity is the contribution of the electron gas $C_e(T) = 7.4 \cdot 10^{-5} T$ (J mol^{-1} K^{-1}). The model parameters obtained in [14] are in a good agreement with Raman scattering data [15].

In this study, using Density Functional Theory (DFT), the electronic, phonon, and thermodynamic properties (specific heat, entropy, free energy and Gibbs energy, temperature dependences of

* Corresponding author.
E-mail address: vvnovikov@mail.ru (V.V. Novikov).

https://doi.org/10.1016/j.jallcom.2020.158020
0925-8388/

the bulk modulus and Grüneisen parameter) of LaB_4 are investigated and the obtained results are compared with experimental data obtained previously [14]. The model for describing the temperature dependence of the heat capacity of LaB_4 (the low-temperature contribution of two-level systems (TLS) was taken into account) is also refined. Moreover, the temperature changes of the Grüneisen parameter is analyzed and the features of the electronic and phonon subsystems of boride using DFT calculations are studied.

2. Computational details

The Vienna Ab-initio Simulation Package (VASP) [16,17] has been employed for density functional theory (DFT) calculations. The Perdew–Burke–Ernzerhof (PBE) [18] parameterization of the generalized gradient approximation (GGA) [19] has selected to describe the exchange and correlation functionals. The projector augmented wave (PAW) [20] method has been also used with 700 eV energy cut off for the electron-ion interaction to deal with the interaction between the ion cores and valence electrons. Moreover, the electron-electron interaction has been considered using the strongly constrained and appropriately normed (SCAN) functional within the meta-Generalized Gradient Approximation (meta-GGA) [21] for electronic properties. The optimizations have been carried out using 6 × 6 × 12 k-points with the gamma centred grid [22]. The ground state geometry of LaB_4 compound has been determined with a force convergence criterion as 10^{-11} eV $Å^{-1}$ and an energy convergence criterion as 10^{-12} eV per unit cell. For the vibrational properties, PHONOPY software [23] has been used for the supercell generation (2 × 2 × 1) and this supercell has been employed to VASP using linear response method.

3. Electronic properties

The crystal structure of LaB_4 has the tetragonal shape with space group P4/mbm (No.127), as shown in Fig. 1. The lanthanum atoms in the crystal structure of LaB_4 occupy the positions La 4 g (x, ½ + x, 0). Three non-equivalent boron atoms occupy the positions B1 4e (0,0, z), B2 4 h (x, ½ + x, 1/2) and B3 8j (x, y, 1/2), respectively. After the geometry optimization in VASP, the crystal structure is fully relaxed and the obtained equilibrium lattice constants are obtained and listed in Table 1. Also, Table 1 lists the experimental data from Ref [24] to compare the obtained results and as can be concluded from the table, the theoretical results are consistent with the experimental ones.

Furthermore, the partial densities of states for LaB_4 (see Fig. 2) have been obtained. As can be seen from this figure, this compound has a metallic nature due having no band gap. The density of states at the Fermi level has been found as $N(E_F) = 0.87\ eV^{-1}$ form $unit^{-1}$.

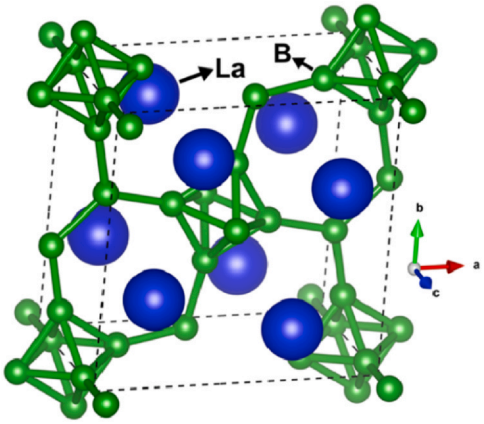

Fig. 1. The crystal structure of LaB_4 in 3D.

Table 1
Lattice constants (*a, and c in* Å) and positions of La and B atoms.

	Experiment [24]	Theoretical
a	7.324	7.309
c	4.181	4.183
La_x	0.3166	0.3163
$B1_z$	0.2088	0.2940
$B2_x$	0.0884	0.0884
$B3_x$	0.1743	0.1735
$B3_y$	0.0394	0.0389

This corresponds to a coefficient of electronic heat capacity (Sommerfeld constant) of $\gamma = 2.05\ mJ\ K^{-2}\ mol^{-1}$, which approximately corresponds to the refined experimental value of $\gamma = 1.85\ mJ\ K^{-2}\ mol^{-1}$.

An analysis of the interatomic interaction for LaB_4 shows that the main types of interactions can be attributed to s and p orbitals of B, p, d, and f orbitals of La (Fig. 2). The more contribution to the partial density of states below the Fermi level comes from the p orbitals of B atoms and there is a hybridization between d orbitals of La atoms and p orbitals of B atoms in the energy range between − 4.3 eV and 0 eV. Moreover, there is a hybridization between f orbitals of La atoms, d orbitals of La atoms and p orbitals of B atoms in the energy range between 1 eV and 4 eV above the Fermi level.

It must be emphasised that this effect is identical for the YB_4 system, as shown in [1]. In addition, to understand the chemical bonding type made by atoms, electronic charge density distributions have been plotted for different plane as shown in Fig. 3. According to these plots, it could be indicated that the bond between boron atoms is of a substantial covalent nature, which determines the stability of the boron sublattice and high strength properties for this system [25].

It can be seen from the band structure of LaB_4 shown in Fig. 4 that electronic levels have a high dispersion. A weakly pronounced feature in the band structure of LaB_4 along the R-A direction is observed due to the broad gap of about 4 eV along the top (and bottom) edges R-A of the Brillouin zone. As seen from the figure, along these edges, lines stick together in pairs and the structure is much less dispersed. This gap closes along the $k_z = \pi/c$ plane of the zone only for small in-plane components of the wave vectors. The gaps enclosing E_{Fermi} often indicates the stability of a crystal structure and the high crystalline stability of lanthanum tetraboride [1].

In addition, the Fermi surface is crucial for the metallic systems and it is a surface that separates the filled and unfilled states in the reciprocal states. Fig. 5 shows the Fermi surface of LaB_4 obtained using DFT where there are 10–13 no. of bands that crosses the Fermi level for LaB_4. In Fig. 5, the empty regions show the holes and the coloured regions show the electrons where the colour changes due the electron velocity. The red colour corresponds to the high velocity while the purple colour represents the low velocity. The other colours correspond to intermediate velocity. The Fermi surface determines the electrical conductivity for the metals and as can be seen from the figure, at the centre of the Brillouin zone (at the Γ point) and at the Z point there are closed surfaces of an electronic type. Also, there are 3D surfaces of complex topology of the hole type along the direction Γ–Z and there are small closed surfaces of a hole type of a fusiform shape along the direction Γ–M.

4. Phonon spectrum and thermodynamic functions of LaB_4

The dynamical stability of a compound could be determined with the phonon dispersion curves. The stability is also of very high importance for evaluating the material stability because the soft phonon modes can reflect the possible distortion in crystal. A stable crystalline structure requires all phonon frequencies and the corresponding phonon DOS to be positive, as seen in Fig. 6, the absence of

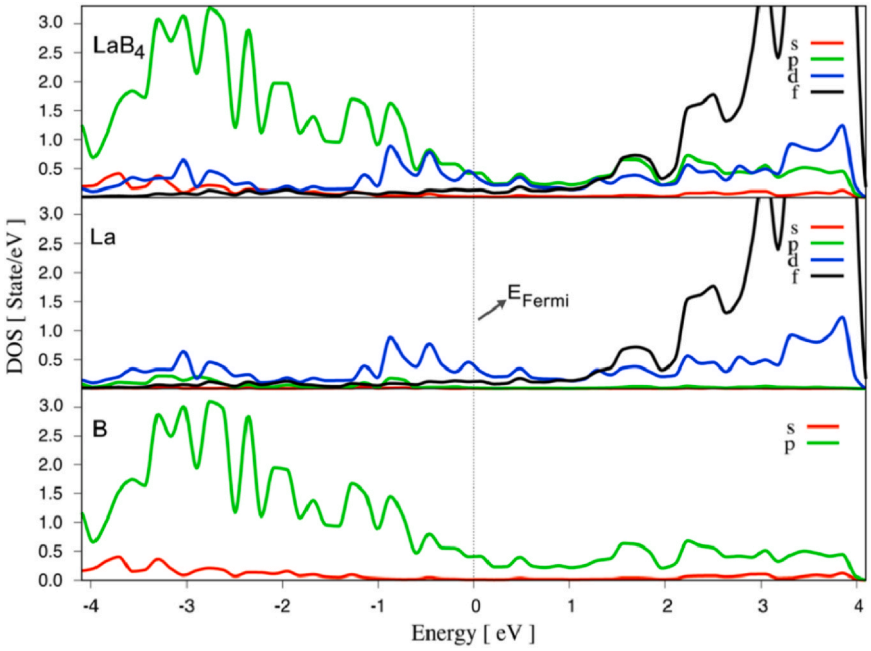

Fig. 2. Partial densities of states of LaB_4.

any imaginary phonon frequency in the whole Brillouin zone for this compound indicates the dynamical stabilities. There are 60 branches in the phonon spectrum consisting of 3 acoustic and 57 optic branches with respect to having 20 atoms in the primitive cell.

The phonon density of states is shown in Fig. 6 where the B atoms give more contribution to the optic modes as shown in Fig. 6 due to the lower atomic mass than La atoms. In addition, this phonon spectrum can be divided by frequency into three areas. The first region (from 0 to 5.3 THz) relates to acoustic phonons and is determined by the contribution of vibrations of La atoms. The second region (from 7.9 to 27.7 THz) related to optical phonons is determined by the vibrational modes of B atoms, which mainly interact with La atoms. The third low-dispersion region (from 30.8 to 32.1 THz) refers to high-frequency optical phonons, which characterise the interaction between the atoms of the B sublattice.

Furthermore, it is well known that the first-principles calculations are limited to calculate thermodynamic properties directly [26,27]. However, the thermodynamic properties could be determined using approximations such as Quasi-harmonic Debye [23] that are based on phonons. Based on the obtained phonon spectrum

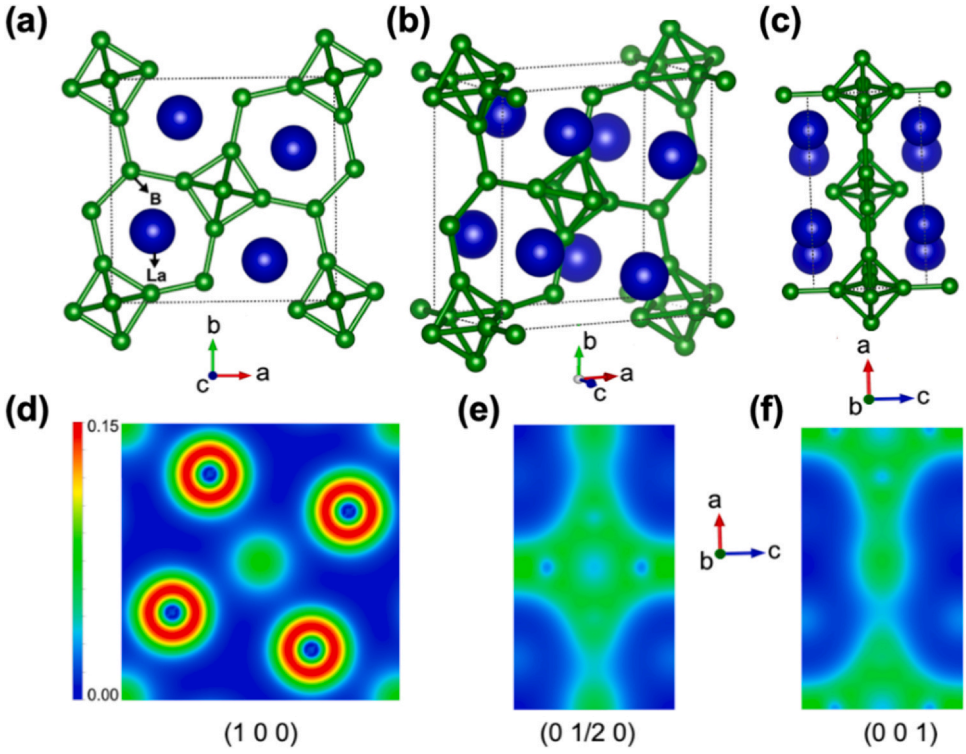

Fig. 3. The crystal structure in (1 0 0) (a), (1 ½ 0) (b) and (0 0 1) (c) orientations and corresponding electronic charge densities (d), (e) and (f), respectively.

of LaB_4, the temperature-dependent Helmholtz free energy F, entropy S, molar heat capacity at constant volume C_v and molar heat capacity at constant pressure C_p [23] has been obtained:

$$F = \frac{1}{2}\sum_{qj}\hbar\omega_{qj} + k_B T\sum_{qj} ln[1 - exp(-\hbar\omega_{qj}/k_B T]$$

$$S = \frac{1}{2T}\sum_{qj}\hbar\omega_{qj} coth[\hbar\omega_{qj}/2k_B T] - k_B\sum_{qj} ln\left[2sinh\left(\frac{\hbar\omega_{qj}}{2k_B T}\right)\right]$$

$$C_V = \sum_{qj} C_{qj} = \sum_{qj} k_B\left(\frac{\hbar\omega_{qj}}{k_B T}\right)^2 \frac{exp(\hbar\omega_{qj}/k_B T)}{[exp(\hbar\omega_{qj}/k_B T) - 1]^2}$$

$$C_P(T, p) = -T\frac{\partial^2 G(T. p)}{\partial T^2} = C_V(T, V(T, p)) + T\frac{\partial V(T, p)}{\partial T}\frac{\partial S(T; V)}{\partial V}\Big|_{V=V(T,p)}$$

where k_B, $\hbar$, and T are the Boltzmann constant, Planck constant and absolute temperature, respectively, and ω_{qj} are the eigenvalues of the dynamic matrix for the wave vector $\boldsymbol{q_j}$.

Fig. 7 shows the experimental and theoretical temperature dependences of the entropy for LaB_4. As can be seen, these dependencies completely coincide, which allows us to use the so-called quasi-harmonic approximation to determine the temperature dependences of the specific heat C_p, Grüneisen coefficient, bulk modulus B, crystal lattice constants and so on.

The temperature dependent entropy has been used to obtain the molar heat capacity that is an important parameter for the technological applications of materials. Fig. 8 shows the experimental and theoretical dependences of the molar heat capacities $C_v(T)$ and $C_p(T)$ for LaB_4. It can be seen that the coincidence of theoretical calculations of heat capacities with experiment is actually absolute.

Next, the theoretical values of the temperature dependence of the Grüneisen parameter γ, the bulk modulus B, Gibbs free energy has been calculated. The calculations of the Grüneisen parameter were performed according to the formulas:

$$\gamma_{qj}(V) = -\frac{V}{2(\omega_{qj})^2}\sum_{\alpha\beta\kappa\kappa'} e_{qj}^{\alpha\kappa *}\frac{\partial D_{\kappa\kappa'}^{\alpha\beta}(V, q)}{\partial V} e_{qj}^{\beta\kappa'}$$

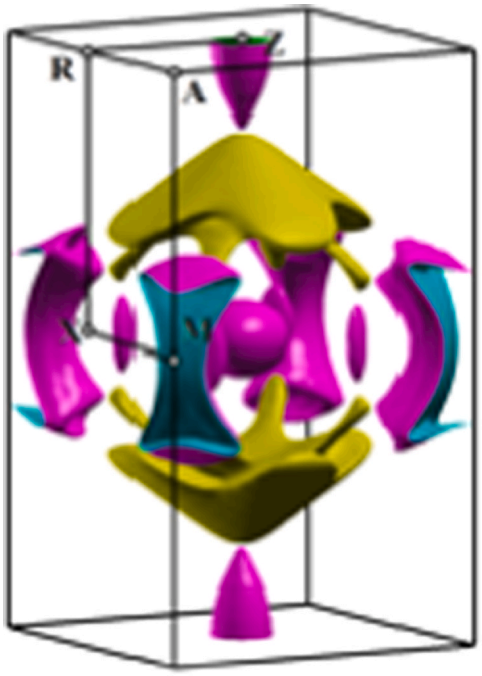

Fig. 5. Fermi surface of LaB_4. (For interpretation of the references to colour in this figure legend, the reader is referred to the web version of this article.)

$$\gamma = \sum_{qj}\gamma_{qj} C_{qj}/C_V$$

where $D_{qj}^{\alpha\beta}$ are the elements of the dynamic matrix and e are the elements of the polarisation vector [17]. Fig. 9 shows the temperature dependence of Grüneisen parameter with the experimental and theoretical results. As can be seen from the figure, both dependences are close and demonstrate a similar character of changes with temperature: in the region of elevated and moderately low temperatures, both curves are located almost horizontally near values 1.2–1.3; with decreasing temperature, an increase in both quantities and a sharp maximum near 15 K are observed. With a further decrease in temperature, the values of $\gamma_{exp}(T)$ and $\gamma_{calc}(T)$ decrease.

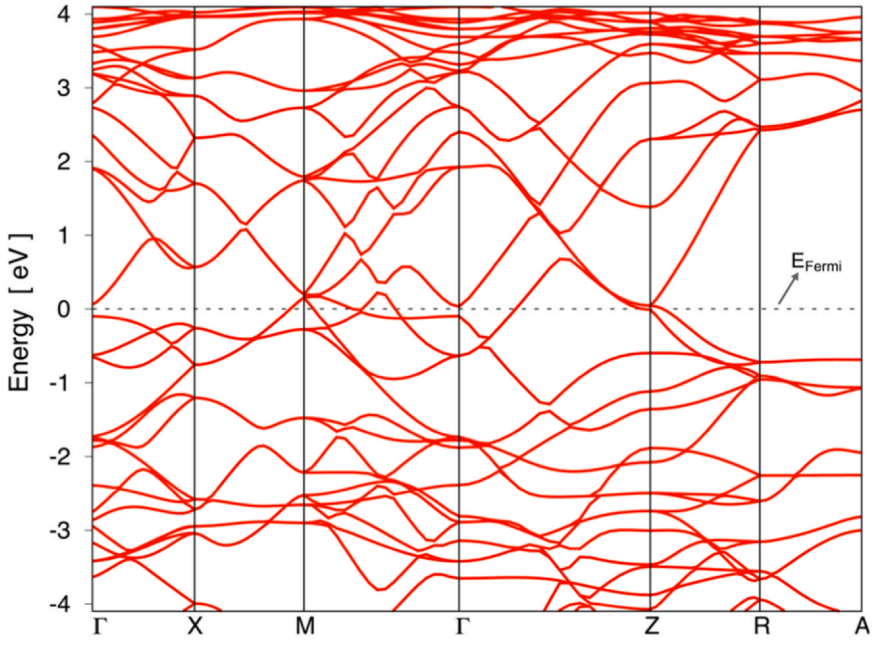

Fig. 4. Band structure of LaB_4.

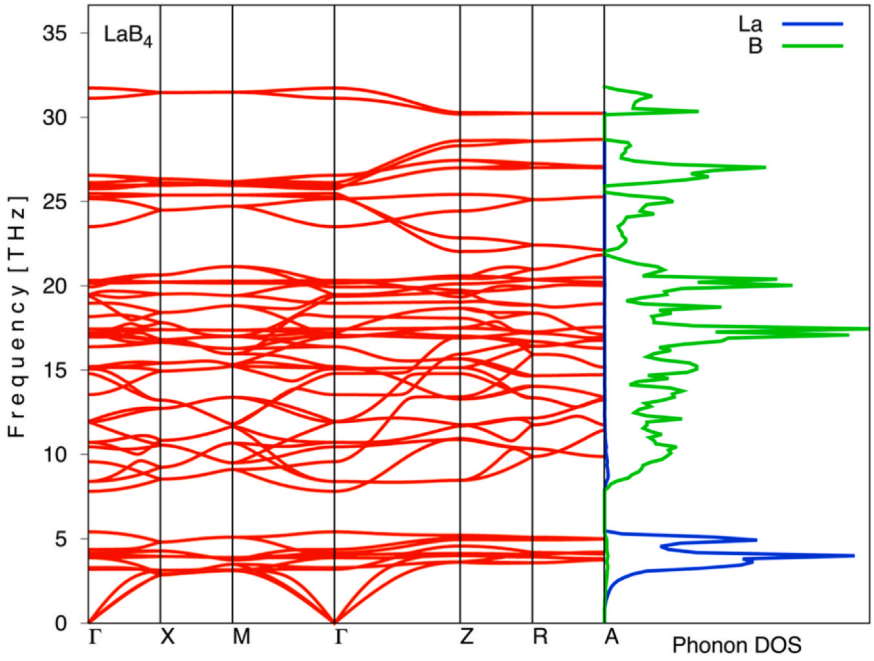

Fig. 6. Dispersion dependence and phonon spectrum of LaB_4.

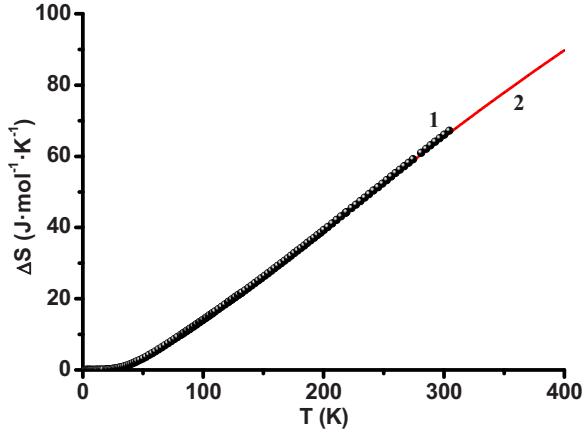

Fig. 7. Experimental (1) and theoretical (2) temperature dependences of the LaB_4 entropy.

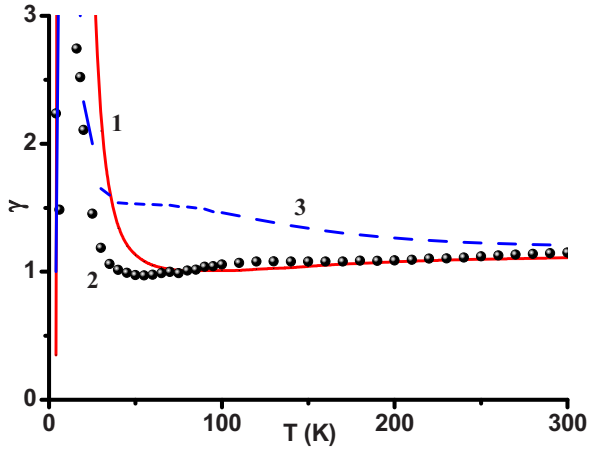

Fig. 9. Dependence of the Grüneisen parameter on temperature: 1–γ (T); 2–γ_{exp}(T); 3–γ_{calc}(T).

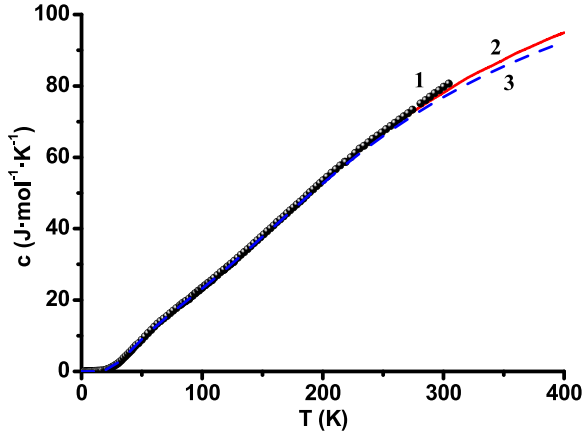

Fig. 8. Experimental (1) and theoretical temperature dependences of C_P (2) and C_V (3).

The values of the bulk modulus of lanthanum tetraboride B_{LaB4}(T) obtained from the calculations (Fig. 10) are close to the data from [28] and are consistent with the data [29] for LuB_4 at room temperature (183.5 GPa). The values of B_{LuB4} and B_{LaB4} are of the same order. Moreover, as one would expect for tetraboride with lower lattice parameters, $B_{LuB4} > B_{LaB4}$.

As can be seen from Fig. 10, the decrease in the total bulk modulus in the range from 0 to 400 K occurs only by 2.6%. This suggests that quantum chemical calculations performed at a temperature of 0 K make it possible to obtain the values of the elastic constants for real operating temperatures with high accuracy comparable to the experimental error.

The detailed experimental and theoretical studies have been performed for the molar heat capacity and thermal expansion coefficient of LaB_4. The molar heat capacity and the thermal expansion coefficient are crucial to provide the thermodynamic characteristic of a material. The experimental temperature dependence of the specific heat $C_{exp}(T)$ in the coordinates C/T^3–T^2 of lanthanum tetraboride [14] is shown in Fig. 11.

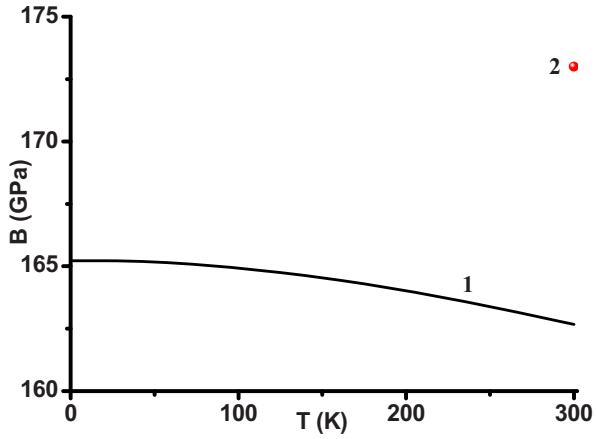

Fig. 10. Temperature dependence of the LaB_4 bulk modulus: 1 – calculation data of the present work; 2 – [28].

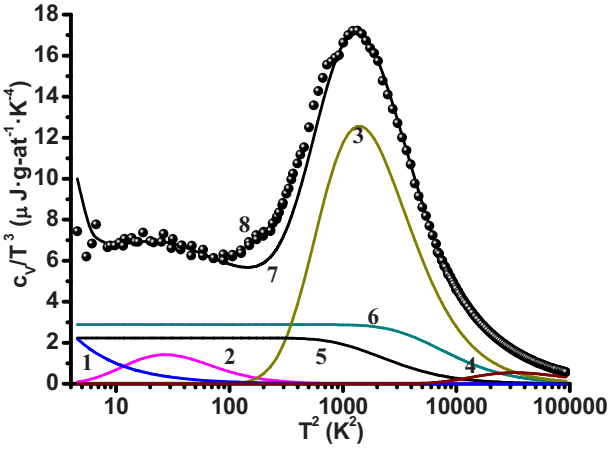

Fig. 11. Heat capacity (C_V/T^3)-(T^2) of lanthanum tetraboride: 1 - electronic component of the specific heat $C_e(T)$; 2 - TLS contribution $C_{TLS}(T)$; 3, 4 - Einstein contributions C_{E1}, C_{E2} (θ_{E1} = 184 K, θ_{E2} = 890 K); 5, 6 - Debye contributions C_{D1}, C_{D2} (θ_{D1} = 230 K, θ_{D2} = 420 K); 7 - $\sum C_i$; 8–$C_{exp}(T)$.

In the present work, when analysing the dependence (C_p/T^3)–(T^2), in contrast to [14], a weak anomaly near 100 K^2 has been taken into account, approximating it by the contribution of TLS $C_{TLS}(T)$ [30] as can be seen from Fig. 11. The environment of lanthanum atoms with boron atoms in the crystal structure of LaB_4 is not spherically symmetric. This asymmetry becomes even greater due to the possible imperfection of the boron sublattice. Therefore, lanthanum atoms have the opportunity to occupy spatially close, but energetically non-equivalent positions in the cavities of the boron matrix, which leads to the formation of TLS. In the C_p/T^3 plot of T^2, the TLS contribution appears as a bell-shaped hill. The dependence $C_{TLS}(T)$ was calculated by the relation:

$$C_{TLS} = \frac{R\left(\frac{\delta}{T}\right)^2 be^{-\frac{\delta}{T}}}{\left(1 + be^{-\frac{\delta}{T}}\right)^2},$$

where R is the universal gas constant, δ is the TLS energy difference in Kelvin and b is the ratio of the degeneracy rates of the excited and ground states [31,32]. In LaB_4 case, it was obtained that $\delta = 45$ K and $b = 0.1$.

The introduction of $C_{TLS}(T)$ into consideration led to a slight change in the parameters of the Debye-Einstein model, with the quantity θ_{E1} having to be increased by 7 K compared with the results of [14]. A comparison of the characteristic Debye and Einstein frequencies obtained from the analysis of $C_p(T)$ data with the LaB_4 phonon spectrum shows their satisfactory mutual correspondence for the interval from low frequencies to moderately high ones.

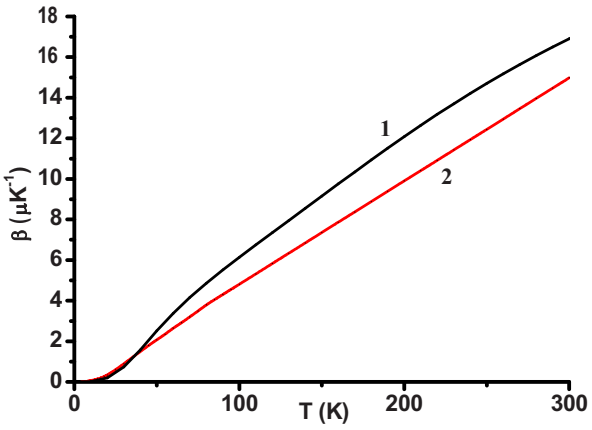

Fig. 12. Volume thermal expansion coefficient of LaB_4: 1–$\beta_{calc}(T)$ [14]; 2–$\beta_{exp}(T)$.

Furthermore, these detailed heat capacity contributions could reveal the low temperature anomaly of the temperature dependence of the Grüneisen parameter. To clarify the causes of the observed low-temperature anomalies in the temperature dependence of the Grüneisen parameter of lanthanum tetraboride, the dependence $\gamma(T)$ as the sum of the contributions of various modes of the phonon spectrum has been presented:

$$\gamma(T) = (\gamma_e C_e + \gamma_{TLS} C_{TLS} + \gamma_{D1} C_{D1} + \gamma_{D2} C_{D2} + \gamma_{E1} C_{E1} + \gamma_{E2} C_{E2})/ (C_e + C_{TLS} + C_{D1} + C_{D2} + C_{E1} + C_{E2}),$$

where C_i are various contributions to the heat capacity of tetraboride (see Fig. 11) and γ_i are the Grüneisen mode parameters corresponding to these contributions (selected by fitting to the experimental data). As a result of the fitting process, it was found that the behaviour of the $\gamma(T)$ curve in the region of elevated and moderately low temperatures (150–300 K) is determined by the high-frequency contributions of Einstein and Debye $C_{D1}(T)$ and $C_{E1}(T)$ (γ_{D1} = 1.2 and γ_{E1} = 1.2). At temperatures of 50–150 K, the quantities $\gamma(T)$ are determined mainly by the influence of the low-frequency components $C_{D2}(T)$ and $C_{E2}(T)$ (γ_{D2} = 1.2, γ_{E2} = 0.8). The sharp increase in the $\gamma(T)$ dependence at temperatures of 10–20 K is caused, as it turned out, by the influence of TLS (γ_{TLS} = 45), and the subsequent decline is due to the influence of free electron gas (γ_e = − 10).

The temperature dependence of the volumetric thermal expansion coefficient ($\beta(T)$) is shown in Fig. 12 for LaB_4. $\beta(T)$ could be determined using

$$\gamma_{exp}(T) = \beta(T)\, B\, V_m/C_v(T)$$

where $\gamma_{exp}(T)$ is the Grüneisen parameter, B is the bulk modulus and V_m is the molar volume. The experimental temperature dependence of LaB_4 volume thermal expansion coefficient $\beta_{exp}(T)$ is compared with calculated one $\beta_{calc}(T)$ in Fig. 12. As can be seen, the difference between these values is less than the experimental error.

5. Conclusion

The possibility of theoretical prediction of the behaviour of the electronic and thermodynamic properties of borides of RB_4 family, the experimental determination of which often requires considerable labour both in the synthesis of objects of study and during the experiment, is shown. At the same time, an experimental study of the behaviour of various boride subsystems when changing external influences provides material that allows us to test theoretical approaches and establish the limits of their applicability.

As a result of the analysis of interatomic interaction, the band structure, the high thermal and mechanical characteristics of tetraborides were first explained. The calculated dispersion curves and the phonon spectrum of lanthanum tetraboride were the theoretical justification for the use of the previously used approaches to the analysis of the experimental temperature dependences of the thermodynamic properties of RE tetraborides, as well as other classes of borides. A detailed analysis of the temperature changes in the thermodynamic characteristics of LaB_4 at the lowest helium temperatures revealed the influence of TLS, the existence of which is due to the features of the crystal structure, as well as a quantitative description of their effect on the behaviour of the phonon subsystem of boride. The results of calculations of the main characteristics of the electronic, phonon and thermodynamic properties subsystems of lanthanum tetraboride by quantum chemical methods have shown satisfactory agreement between the calculated and experimental values in a wide low-temperature region.

CRediT authorship contribution statement

Haci Ozısık: Data curation, Conceptualization, Methodology, Software. **Gokhan Surucu**: Methodology, Software, Writing - original draft preparation. **Engin Deligoz**: Writing - review & editing. **Igor Shein**: Data curation, Writing - original draft preparation. **Aleksandr Matovnikov**: Visualization, Investigation. **Nikolay Mitroshenkov**: Visualization, Investigation. **Anton Morozov**: Software, Validation. **Vladimir Novikov**: Supervision.

Declaration of Competing Interest

The authors declare that they have no known competing financial interests or personal relationships that could have appeared to influence the work reported in this paper.

Acknowledgements

This study was supported by the Russian Foundation for Basic Research and the Administration of the Bryansk Region of the Russian Federation (grant No. 18-42-320001 r-a).

References

[1] Z.P. Yin, W.E. Pickett, Rare-earth–boron bonding and 4f state trends in RB_4 tetraborides, Phys. Rev. B 77 (2008) 035135.
[2] G. Will, W. Shäfer, F. Pfeiffer, F. Elf, J. Eautrneau, Neutron diffraction studies of TbB_4 and ErB_4, J. Less Common Met. 82 (1981) 349–355.
[3] G.A. Wigger, E. Felder, R. Monnier, H.R. Ott, Low-temperature phase transitions in the induced-moment system PrB_4, Phys. Rev. B 72 (2005) 014419014419-8.
[4] R. Watanuki, T. Kobayashi, R. Noguchi, K. Suzuki, J. Phys. Conf. Ser. 150 (2009) 042229-4.
[5] S. Yoshil, T. Yamamoto, M. Hagiwara, S. Michimura, A. Shigekawa, F. Iga, T. Takabatake, K. Kiuda, Multistep magnetization plateaus in the shastry-sutherland system TbB_4, Phys. Rev. Lett. 101 (2008) 087202–087204.
[6] V.V. Novikov, N.V. Mitroshenkov, A.V. Matovnikov, D.V. Avdashchenko, S.V. Trubnikov, A.V. Morozov, Peculiarities of the lattice thermal properties of rare-earth tetraborides, J. Therm. Anal. Calorim. 120 (2015) 1597–1602.
[7] V.V. Novikov, A.V. Morozov, A.V. Matovnikov, D.V. Avdashchenko, Ya.N. Polesskaya, N.V. Sakhoshko, B.I. Kornev, V.D. Solomennik, V.V. Novikova, Low-temperature heat capacity of rare-earth tetraborides, Phys. Solid State 53 (2011) 1839–1844.
[8] V.V. Novikov, N.V. Mitroshenkov, A.V. Morozov, A.V. Matovnikov, D.V. Avdashchenko, Heat capacity and thermal expansion of gadolinium tetraboride at low temperatures, J. Appl. Phys. 111 (2012) 063907.
[9] B.S. Shastry, B. Sulherland, Exact ground state of a quantum mechanical antiferromagnet, Phys. B+C 108 (1981) 1069–1070.
[10] T. Matsumura, D. Okuyama, H. Nakao, Y. Murakami, Phot. Fact. Act. Rep. 23 (2005) 116.
[11] S. Michimura, A. Shigekawa, F. Iga, M. Sera, T. Takabatake, K. Ohoyama, Y. Okabe, Magnetic frustrations in the Shastry–Sutherland system ErB_4, Phys. B Condens. Matter 378–380 (2006) 596–597.
[12] K. Siemensmeyer, E. Wulf, H.-J. Mikeska, K. Flachbart, S. Gabani, S. Mat`as, P. Priputen, A. Efdokimova, N. Shitsevalova, Fractional magnetization plateaus and magnetic order in the Shastry-Sutherland magnet TmB_4, Phys. Rev. Lett. 101 (2008) 177201–177204.
[13] V.V. Novikov, A.V. Matovnikov, N.V. Mitroshenkov, A.K. Tolstosheev, The residual entropy of Shastry-Sutherland lattice of rare-earth tetraborides, J. Alloys Compd. 666 (2016) 98–100.
[14] V.V. Novikov, N.V. Mitroshenkov, A.V. Matovnikov, Peculiarities of electronic, phonon and magnon subsystems of lanthanum and samarium tetraborides, J. Alloys Compd. 646 (2015) 906–911.
[15] H. Werheit, V. Filipov, N. Shitsevalova, M. Armbrűster, U. Schwarz, A. Ievdokimova, V. Muratov, V. Gurin, M. Korsukova, Raman scattering in rare earths tetraborides, Solid State Sci. 31 (2014) 24–32.
[16] G. Kresse, J. Furthmüller, Efficient iterative schemes forab initiototal-energy calculations using a plane-wave basis set, Phys. Rev. B 54 (1996) 11169–11186.
[17] G. Kresse, D. Joubert, From ultrasoft pseudopotentials to the projector augmented-wave method, Phys. Rev. B 59 (1999) 1758–1775.
[18] J.P. Perdew, K. Burke, M. Ernzerhof, Generalized gradient approximation made simple, Phys. Rev. Lett. 77 (1996) 3865–3868.
[19] G. Kresse, J. Furthmuller, Efficiency of ab-initio total energy calculations for metals and semiconductors using a plane-wave basis set, Comput. Mater. Sci. 6 (1996) 15–50.
[20] P.E. Blöchl, Projector augmented-wave method, Phys. Rev. B 50 (1994) 17953–17979.
[21] J. Sun, R.C. Remsing, Y. Zhang, Z. Sun, A. Ruzsinszky, H. Peng, Z. Yang, A. Paul, U. Waghmare, X. Wu, M.L. Klein, J.P. Perdew, Accurate first-principles structures and energies of diversely bonded systems from an efficient density functional, Nat. Chem. 8 (2016) 831–836.
[22] J.D. Pack, H.J. Monkhorst, Special points for Brillouin-zone integrations"—a reply, Phys. Rev. B 16 (1977) 1748–1749.
[23] A. Togo, I. Tanaka, First principles phonon calculations in materials science, Scr. Mater. 108 (2015) 1–5.
[24] K. Kato, I. Kawada, C. Oshima, C. Oshima, S. Kawai, Lanthanum tetraboride, Acta Crystallogr. Sect. B Struct. Crystallogr. Cryst. Chem. 30 (1974) 2933–2934.
[25] G. Surucu, B. Yildiz, A. Erkisi, X. Wang, O. Surucu, The investigation of electronic, anisotropic elastic and lattice dynamical properties of MAB phase nanolaminated ternary borides: M_2AlB_2 (M = Mn, Fe and Co) under spin effects, J. Alloys Compd. 838 (2020) 155436.
[26] H.B. Ozisik, K. Colakoglu, G. Surucu, H. Ozisik, Structural and lattice dynamical properties of Zintl NaIn and NaTl compounds, Comput. Mater. Sci. 50 (2011) 1070–1076.
[27] G. Surucu, K. Colakoglu, E. Deligoz, N. Korozlu, H. Ozisik, Thermo-elastic and lattice dynamical properties of Rh_3Hf compound, Comput. Mater. Sci. 48 (2010) 859–865.
[28] M. de Jong, W. Chen, T. Angsten, A. Jain, R. Notestine, Charting the complete elastic properties of inorganic crystalline compounds, Sci. Data 2 (2015) 150009.
[29] E. Deligoz, H. Ozisik, K. Colakoglu, G. Surucu, Y.O. Ciftci, Mechanical and phonon properties of the superhard LuB_2, LuB_4, and LuB_{12} compounds, J. Alloys Compd. 509 (2011) 1711–1715.
[30] V.V. Novikov, K.S. Pilipenko, A.V. Matovnikov, N.V. Mitroshenkov, M.S. Likhanov, A.S. Tyablikov, A.V. Shevelkov, Effect of the cation sublattice composition of tin-based type-I clathrates on their low-temperature thermal properties, Dalton Trans. 47 (2018) 11219–11225.
[31] R. Karlin, Magnetochemistry, Springer-Verlag,, Berlin-Heidelberg-New York-Tokyo, 1986.
[32] V.V. Novikov, D.V. Avdashchenko, S.L. Bud'ko, N.V. Mitroshenkov, A.V. Matovnikov, H. Kim, M.A. Tanatar, R. Prozorov, Spin glass and glass-like lattice behaviour in HoB_{66} at low temperatures, Philos. Mag. 93 (2013) 1110–1123.